ORIGINAL ARTICLE

Revisiting the Intrabinary Shock Model for Millisecond Pulsar Binaries: Radiative Losses and Long-Term Variability

Jaegeun Park¹ | Chanho Kim¹ | Hongjun An¹ | Zorawar Wadiasingh^{2,3,4}

¹Department of Astronomy and Space Science, Chungbuk National University, Cheongju 28644, Republic of Korea

- ²Department of Astronomy, University of Maryland College Park, MD 20742, USA
- ³Astrophysics Science Division, NASA GSFC, MD 20771, USA
- ⁴Center for Research and Exploration in Space Science and Technology, NASA GSFC, MD 20771, USA

Correspondence

*Hongjun An, Department of Astronomy and Space Science, Chungbuk National University, Cheongju 28644, Republic of Korea. Email: hjan@cbnu.ac.kr

Funding Information

Ministry of Education, RS-2023-00274559. Korean Government (MSIT), NRF-2023R1A2C1002718.

Spectrally hard X-ray emission with double-peak light curves (LCs) and orbitally modulated gamma rays have been observed in some millisecond pulsar binaries, phenomena attributed to intrabinary shocks (IBSs). While the existing IBS model by Sim, An, and Wadiasingh (2024) successfully explains these high-energy features observed in three pulsar binaries, it neglects particle energy loss within the shock region. We refine this IBS model to incorporate radiative losses of X-ray emitting electrons and positrons, and verify that the losses have insignificant impact on the observed LCs and spectra of the three binaries. Applying our refined IBS model to the X-ray bright pulsar binary PSR J1723–2837, we predict that it can be detected by the Cherenkov Telescope Array. Additionally, we propose that the long-term X-ray variability observed in XSS J12270–4859 and PSR J1723–2837 is due to changes in the shape of their IBSs. Our modeling of the X-ray variability suggests that these IBS shape changes may alter the extinction of the companion's optical emission, potentially explaining the simultaneous optical and X-ray variability observed in XSS J12270–4859. We present the model results and discuss their implications.

KEYWORDS:

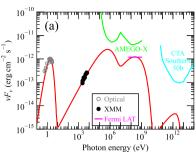
pulsars: individual (XSS J12270–4859, PSR J1723–2837), X-rays: binaries, gamma rays: theory, radiation mechanism: non-thermal

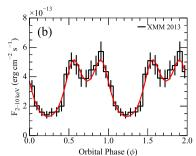
1 | INTRODUCTION

Millisecond pulsar binaries, hosting a millisecond pulsar and a low-mass companion, form after a long period of accretion from the companion ceases. This accretion phase spins up the neutron star to millisecond periods (Alpar, Cheng, Ruderman, & Shaham, 1982) and can significantly increase its mass (e.g., van Kerkwijk, Breton, & Kulkarni, 2011). Therefore, pulsar binaries serve as invaluable probes for studying the evolution of low-mass X-ray binaries and constraining the equation of state of dense matter (e.g., Linares, 2020). To fully exploit their potential, a comprehensive understanding of the pulsar-companion interaction and accurate determination of system

parameters, such as orbital inclination, through broadband emission modeling are essential.

Observationally, compact millisecond pulsar binaries are categorized into black widows (BWs) and redbacks (RBs) depending on the companion's mass (M_c); BWs have $M_c < 0.1 M_{\odot}$, and RBs have $M_c > 0.1 M_{\odot}$ (see Strader et al., 2019; Swihart et al., 2022). BWs and RBs share similar emission properties, most notably the prominent orbital modulation across multiple wavelengths. Some systems undergo radio eclipses caused by the companion's outflow at specific orbital phases. In the optical band, the characteristic day-night cycles arise from the pulsar's heating of the companion and ellipsoidal modulation. These systems display hard power-law (PL) X-ray emission (photon index $\Gamma \approx 1.2$) with orbital modulation, typically characterized by a single or double-peak light curve (LC). The X-ray emission peaks around orbital phase





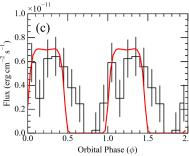


FIGURE 1 Spectral energy distribution (SED) and light curves (LCs) of XSS J12270–4859 (Sim et al., 2024). (a): SED displaying blackbody emission from the companion (gray), and non-thermal X-ray data (black). Estimated flux of the orbitally modulated \le GeV signal is indicated by the pink line. Green and cyan curves show the sensitivity of the AMEGO-X and CTA observatories. (b): X-ray LC in the 2–10 keV band measured by XMM-Newton. (c) 100 MeV-1 GeV LC measured by Fermi LAT (An, 2022). The red curves present our model (Table 1).

 $\phi \approx 0.75$ or $\phi \approx 0.25$ depending on the IBS orientation, where $\phi \approx 0.75$ denotes the phase when the companion is behind the pulsar as seen by the observer. These phenomena allow us to study the pulsar wind and its interaction with the companion's wind or magnetic field (e.g., Harding & Gaisser, 1990; Wadiasingh, Venter, Harding, Böttcher, & Kilian, 2018).

Previously, gamma-ray emission from these systems was thought to arise from the pulsar magnetosphere (i.e., pulsed). However, recent Fermi-LAT detections of orbitally modulated SeV signals in a few systems challenge this notion (e.g., An, Romani, & Kerr, 2018; Ng, Takata, Strader, Li, & Cheng, 2018). These signals reach $\approx 30\%$ of the pulsed magnetospheric flux, with a LC maximum at $\phi \approx 0.25$. Moreover, there is evidence suggesting that these orbitally modulated signals may be pulsed and have spectra distinct from the pulsar's emission (An, Romani, & Kerr, 2020; Clark et al., 2021). A comprehensive study of this high-energy emission, employing a suitable emission model, could provide crucial insights into the energetic processes within these systems. Such an investigation might shed light on the origin of the recently detected positron excess (Linares & Kachelrieß, 2021) and elucidate the physical mechanisms operating in more energetic TeV gamma-ray binaries (e.g., Kim, An, & Mori, 2022).

This paper investigates the high-energy emission properties of RBs. Section 2 presents a model for high-energy emission in these systems. In Section 3, we apply our IBS model to the LCs and spectral energy distributions (SEDs) of a sample of RBs (Section 3.1). Additionally, we model the long-term X-ray variability observed in PSR J1723–2837 and XSS J12270–4859 (J1723 and J1227 hereafter; Section 3.2). Finally, Section 4 discusses our results.

2 | A MODEL FOR THE X-RAY AND GAMMA-RAY EMISSION

Previous IBS models (e.g., Kandel, Romani, & An, 2019) primarily focus on X-ray emission. These models postulate that relativistic electrons and positrons (hereafter referred to as

"electrons") are accelerated by the IBS. These particles flow along the shock, emitting radiation that is Doppler-boosted in the direction of their motion, creating a bright ring-like emission region (e.g., Romani & Sanchez, 2016). When the observer's line of sight (LoS) intersects this ring, an X-ray intensity peak is observed. The X-ray LC peak at $\phi \approx 0.75$ commonly observed for RBs (Fig. 1 (b)) suggests that the IBS is bent towards the pulsar in RBs, leading to the strongest Doppler beaming at this orbital phase (e.g., Wadiasingh, Harding, Venter, Böttcher, & Baring, 2017).

Orbitally modulated GeV emission from RBs remains poorly understood. Proposed origins include the pre-shock pulsar wind and the IBS. Synchrotron radiation from the IBS struggles to reproduce the observed GeV LC phasing, while inverse-Compton (IC) emission from the IBS predicts a peak in the SED at TeV energies, inconsistent with observations. Alternatively, IC emission from the pre-shock pulsar wind could explain the GeV LC shape, but this component cannot explain the observed flux levels (An et al., 2020; Clark et al., 2021). Furthermore, these scenarios cannot account for the possible "pulsations" in the orbitally-modulated emission since their emission timescales are longer than the pulse periods of a few milliseconds.

To address the challenges in explaining orbitally modulated GeV emission, van der Merwe, Wadiasingh, Venter, Harding, and Baring (2020) proposed a scenario where high-energy electrons from the pulsar wind have a large gyro radius (greater than the IBS thickness), traverse the IBS, and interact with the companion's strong magnetic field (B) of \sim kG. Sim et al. (2024) (SAW24 hereafter) adopted this 'shock-penetration' scenario. In this framework, rapid energy losses of high-energy electrons $(\propto B^2 E^2)$ due to the companion's strong B is the key factor that generates \leq GeV emission and its orbital modulation. Consequently, SAW24 carefully considered cooling of the shock-penetrating electrons. While successfully reproducing observational data for three RBs, the SAW24 model neglected radiative cooling of electrons within the IBS itself, assuming

that it is insignificant for these systems. However, such cooling could potentially modify the energy distribution of the highest-energy electrons within the IBS, thereby affecting the resulting X-ray spectrum and associated IC emission in the TeV band.

To incorporate radiative cooling within the IBS, we refined the multi-zone IBS model of SAW24. Unlike SAW24, which assumed a stationary electron distribution throughout the IBS, we dynamically updated the distribution in each zone to account for radiative cooling. Cooled particles were then transferred to the subsequent emission zone, and this process was iterated along the electron flow through the IBS.

3 | APPLICATION OF THE MODEL

We apply our updated model to the three RBs used by SAW24, as well as to the X-ray bright RB J1723 (Section 3.1). Additionally, we interpret the long-term X-ray variability observed in J1227 and J1723 within the framework of our IBS model (Section 3.2). We then propose a scenario to explain optical variability in J1227 that was contemporaneous with the long-term X-ray variability (Section 3.3).

3.1 | Broadband SEDs and Multi-band LCs

Figure 1 presents model results for J1227 as an example. Our results for the three RBs modeled by SAW24 are consistent with their findings, suggesting that radiative cooling within the IBS has a negligible impact on the observed LCs and SEDs. This is likely due to the limited energy range of current high-energy observatories, which do not cover energies where the most energetic electrons predominantly emit. A high-quality spectrum extending to higher energies (e.g., by AMEGO-X; Caputo et al., 2022) might reveal the cooling effect.

A particularly interesting case is the bright RB J1723. Its X-ray spectrum, measured by NuSTAR up to 79 keV, exhibits a single PL with $\Gamma=1.3$. Its LC displays a single peak at $\phi=0.75$ (Kong et al., 2017). While GeV emission from this source has been reported (Hui et al., 2014), its origin remains uncertain due to absence of detected pulsations or orbital modulation. van der Merwe et al. (2020) proposed two possible scenarios for this source. In the first, synchrotron radiation from the IBS produces only X-rays, assuming the reported GeV detection is spurious. Alternatively, the IBS could generate both X-ray and GeV photons, requiring strong Doppler beaming for synchrotron emission in the GeV band. A similar scenario has been proposed for the BW PSR J1311–3430 (An, Romani, Johnson, Kerr, & Clark, 2017).

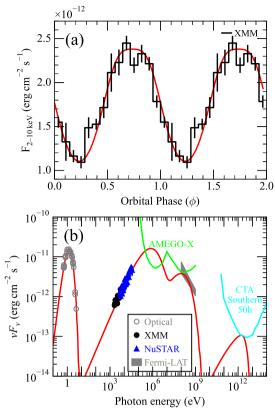


FIGURE 2 X-ray LC and broadband SED of J1723. (a) X-ray LC obtained with XMM-Newton in 2011 (Bogdanov et al., 2014). (b) Companion emission is represented by gray points. X-ray spectra were measured by XMM-Newton (black circles) and NuSTAR (blue triangles) (Kong et al., 2017), and Fermi-LAT data are shown as a gray band (Hui et al., 2014). Red curves in both panels represent our model computations (Table 1), while the sensitivity curves for AMEGO-X and CTA are as presented in Figure 1.

Given the similarities in the X-ray SED and LC phasing between J1723 and other RBs, we employed the scenario where X-rays originate from the IBS and gamma rays from the companion zone. Figure 2 presents the model results. To explore a limiting case, we assumed no magnetospheric contribution to the GeV flux. This assumption directly influences the parameters for shock-penetrating electrons and the companion's B. In reality, the magnetospheric component may contribute up to \sim 70% of the GeV flux, as observed in other RBs, requiring a correspondingly reduced contribution from shock-penetrating electrons. Our model can accommodate lower gamma-ray flux, including nondetection, by adjusting the number of penetrating particles or the companion's B, without altering the IBS or pre-shock parameters (Table 1).

3.2 | Modeling Long-term X-ray variability

Several RBs exhibit pronounced long-term variability in their X-ray emission. Figure 3 presents X-ray LCs of the RBs J1227 (a) and J1723 (b), obtained with XMM-Newton and Chandra at different epochs (Bogdanov et al., 2014; de Martino et al., 2015). A significant variation in X-ray flux

¹This source is not listed in the 4FGL catalog, making the claimed LAT detection less secure.

TABLE 1 Parameters used for models displayed in Figures 1 –3				
Property	Symbol	Unit	J1723	J1227
Basic parameters				
Spin-down power	$\dot{E}_{ m SD}$	$10^{34} \text{ erg s}^{-1}$	4.6	9.0
Orbital period	P_{-}	day	0.615	0.288
Reference Time	$T_{\substack{ ext{asc} \ i}}^{B}$	MJD	55425.3205	57139.0716
Orbital inclination	i	degree	35	54.5
Orbit radius	$a_{\rm orb}$	10^{11}cm	2.6	1.5
Companion mass	M_c	M_{\odot}	0.4	0.27
Companion radius	R_c	$\stackrel{R_{\odot}}{ ext{K}}$	1	0.29
Companion temperature	$rac{R_c}{T_{ m c}}$		5300	5700
Pre-shock parameters				
Pair multiplicity in pre-shock wind	$\mathcal M$	10^{3}	2	2
e ⁻ energy in pre-shock wind	γ_w	10^{4}	7	7
Fraction of spin-down power in pre-shock wind	η_w		0.95	0.95
IBS parameters				
Momentum flux ratio	β		$0.20 (0.36)^{a}$	$0.16 (0.3)^a$
Index for PL distribution of IBS e ⁻	p_1		1.3	1.3
Minimum Lorentz factor of IBS e ⁻	$\gamma_{s,\min}$		1	1
Maximum Lorentz factor of IBS e ⁻	$\gamma_{s,\max}$	10^{7}	1	1
Fraction of spin-down power contained in IBS <i>e</i> ⁻	η_s		0.89	0.92
B within IBS	B_{s}	G	2.66	1.9
Bulk Lorentz factor of the IBS flow	$\Gamma_{\mathrm{D}}^{"}$		1.2	1.5
Length of IBS	l_{sh}	$a_{ m orb}$	4	4
Parameters for emission from the companion zone (shock-penetrating e^-)				
Companion B	\boldsymbol{B}_c	kG	0.14	2.3
Fraction of spin-down power in penetrating e^-	$\eta_T \ \zeta$		0.95	0.95
Penetration efficiency	ζ	_	0.06	0.03
Maximum Lorentz factor of penetrating e^-	γ_p	10^{7}	7	7
Size of the companion zone	$l_{\rm comp}$	$a_{ m orb}$	4	4

TABLE 1 Parameters used for models displayed in Figures 1 -3

Note. For a detailed explanation of how these parameters are employed within the IBS model, please refer to SAW24.

is evident between the two epochs for both sources. In the case of J1227, the change in X-ray flux was accompanied by a corresponding variation in the optical flux (Fig. 3 (c); Section 3.3).

The observed X-ray variability implies changes in the properties of the IBS formed by the interaction between the pulsar and companion winds (e.g., An & Romani, 2017). Given the generally stable nature of pulsar winds, variations in the companion's wind properties are the likely cause of IBS changes. This can affect the momentum flux ratio (β) between the stellar and pulsar winds, defined as:

$$\beta = \frac{\dot{E}_{\rm SD}}{\dot{M}_{w}v_{w}c},\tag{1}$$

where \dot{M}_w is the companion's mass-loss rate, v_w is the wind velocity, and c is the speed of light. The parameter β plays a crucial role in determining the location of the IBS within the system (Fig. 3 (d)).

The parameter β influences the X-ray emission through two primary mechanisms: (1) a smaller β positions the IBS closer to the pulsar, resulting in a stronger B within the shock, as B is primarily supplied by the pulsar and scales inversely with distance from the pulsar to the emission zone $(r_p; \text{Fig. 3} \text{ (d)})$. (2) The IBS opening angle θ_{IBS} decreases with decreasing β values (Canto, Raga, & Wilkin, 1996):

$$\theta_{\rm IBS} - \tan \theta_{\rm IBS} = \frac{\pi}{1 - \beta}.$$
 (2)

The Doppler boosting of IBS emission depends on the angle (Θ) between the IBS flow (approximated by $\theta_{\rm IBS}$) and the LoS. Since the observer's inclination angle (i) remains relatively constant over long timescales, variations in $\Theta (\approx \theta_{\rm IBS} - \pi/2 + i)$ are primarily driven by changes in β through Equation (2). Our modeling indicates that the impact of B on X-ray emission is more significant than that of Doppler boosting due to the relatively low flow speeds $(c\sqrt{1-1/\Gamma_{\rm D}^2};{\rm Table~1~})$ within the IBSs of RBs and limited variation in $\theta_{\rm IBS}$. Consequently, lower- β IBSs generally produce brighter X-ray emission.

We applied our model to investigate the observed long-term X-ray variability in J1227 and J1723. Using parameter values from Table 1 , we initially modeled the brighter (blue) LCs in Figure 3 (a) and (b). To reproduce the lower-flux LCs (red in the figure), we adjusted the β parameter (presented in parentheses in the table). As previously discussed, a strong stellar wind (low β) positions the IBS closer to the pulsar, resulting in a higher B within the shock and enhanced X-ray emission. Conversely, a weaker stellar wind (high β) moves the IBS away from the pulsar (Fig. 3 (d)), reducing X-ray emission. To reproduce the measured LC variabilities, the model requires stellar wind variations of a factor of $\lesssim 2$.

^aNumbers in parentheses refer to the high- β IBS, corresponding to the low X-ray flux LCs (red) in Figure 3 (see Sections 3.2 and 3.3).

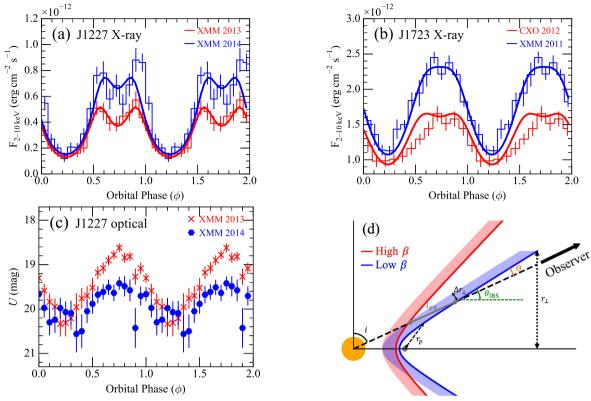


FIGURE 3 (a–b) 2–10 keV LCs of J1227 (a) and J1723 (b) measured by XMM-Newton and Chandra at different epochs (Bogdanov et al., 2014; de Martino et al., 2015). Blue and red curves represent our IBS model. (c) Optical (U band) LCs of J1227 corresponding to the X-ray LCs in panel (a). (d) Schematic illustration of high- β (red) and low- β (blue) IBS configurations at $\phi = 0.75$. Only the low- β IBS includes labels (e.g., θ_{IBS} and r_{\perp}) for clarity. Red and blue regions indicate stellar wind shocks for high- and low- β cases, respectively.

3.3 | Simultaneous Optical and X-ray Variability in J1227

Another intriguing aspect revealed by XMM-Newton's simultaneous X-ray and optical observations of J1227 is the observed anti-correlation between the long-term fluxes in these two wavebands (Fig. 3 (a) and (c)). de Martino et al. (2015) proposed that long-term variations in optical emission could be linked to changes in shock size. A larger shock might produce stronger X-ray modulation while simultaneously causing extinction of some optical light from the companion. However, our IBS model presents challenges for this scenario, as a wider IBS would typically result in weaker X-ray emission.

We propose an alternative explanation for the anti-correlated X-ray and optical variability observed in J1227. Rather than attributing this behavior to the shock region blocking the optical emission, we suggest that the depth (l_{BB}) of the stellar-wind shock traversed by the companion's blackbody photons is crucial (Fig. 3 (d)). The parameter l_{BB} reaches its maximum at $\phi=0.75$ (optical maximum) and is 0 at $\phi=0.25$. For a given shock thickness (Δr_{\perp}), l_{BB} scales with Θ as $l_{BB}\sin\Theta\approx\Delta r_{\perp}$. The number of hydrogen atoms injected during a particle residence time τ_r ($\approx l_{sh}/v_w$ with l_{sh} being the IBS length) within the shock is $N_{\rm H}=\dot{M}_w\tau_r f_{\Omega}/m_{\rm H}$, where $f_{\Omega}=(1-\cos\theta_{\rm IBS})/2$ takes into account the solid angle subtended by the shock from

the companion, and $m_{\rm H}$ is the hydrogen mass. The volume of the stellar-wind shock is approximated as $V_S \approx \pi r_{\perp} l_{sh} \Delta r_{\perp}$ with $r_{\perp} = l_{sh} {\rm sin} \theta_{\rm IBS}$ (assuming a cone). The neutral hydrogen column density along l_{BB} can then be estimated as

$$n_{\rm H} = \frac{N_{\rm H} l_{BB}}{V_S} \approx \frac{\dot{M}_w f_{\Omega}}{\pi m_{\rm H} v_w l_{sh} {\rm sin} \theta_{\rm IBS} {\rm sin} \Theta}. \tag{3}$$

Equation (3) demonstrates that variations in the companion's wind (i.e., $\dot{M}_{w}v_{w}$) can substantially affect the extinction $(A_V \propto n_H; \text{ Diplas & Savage, 1994})$ of the its emission. This is because the wind influences β (Eq. (1)), θ_{IBS} (Eq. (2)) and Θ . For small values of Θ (e.g., Fig. 3 (d)), the $\sin\Theta$ term dominates. Consequently, even a slight change in Θ can lead to a substantial alteration in extinction. Then, the large change in β (and Θ) inferred from the X-ray variability in J1227 between 2013 and 2014 (Table 1) and Section 3.2) offers a qualitative explanation for the observed difference in the U-band magnitudes at $\phi = 0.75$ (Fig. 3 (d)) between the two epochs, although changes in individual \dot{M}_w and v_w may complicate the estimation of A_V . The consistent minimum optical flux (at $\phi =$ 0.25) in both years further supports this scenario, as the shock does not obstruct the companion at that phase. Moreover, this model naturally explains the observed anti-correlation between the long-term optical and X-ray flux variations.

4 | DISCUSSION AND SUMMARY

We refined the IBS model of SAW24 by incorporating the dynamic evolution of electrons within the shock due to radiative cooling. Consequently, the electron spectrum exhibits a lower cutoff energy than that predicted by the SAW24 model, yet this cutoff remains beyond the reach of current high-energy observatories. As a result, this refinement had a negligible impact on the previously reported results for three RBs. Similar to the SAW24 model, our model successfully explains the high-energy emission from the RBs if pulsar wind electrons possess energies of ~40 TeV, penetrate the IBS, and interact with the companion's magnetosphere. While the required voltage drop ($\Delta V \approx 6.6 \times 10^{12} B_{12} P^{-2}$ volts; Ruderman & Sutherland, 1975) is achievable by the millisecond pulsars in those RBs, further theoretical investigation into the dynamics and propagation of such high-energy particles to the companion region is necessary.

Our model results for J1723 are very similar to those of van der Merwe et al. (2020), who attributed its X-ray (and GeV) emission to synchrotron radiation from the IBS. However, a significant discrepancy arises in the TeV band, where our model predicts an order of magnitude lower flux than van der Merwe et al. (2020). This difference stems from our assumption of a larger IBS length, resulting in a greater average distance between TeV-emitting electrons and the companion, and consequently a lower seed photon density within the emission region. Future TeV observations can differentiate between these models, providing crucial insights into the IBS length.

We successfully modeled the long-term X-ray variability observed in J1227 and J1723 by attributing it to variations in the β parameter driven by changes in the stellar wind. These changes also induce variation of l_{BB} (and A_V), causing variability in the observed optical flux. While this simplified model captures the main features of the observed long-term X-ray and optical variability, a more comprehensive treatment incorporating the full IBS geometry is required to accurately fit the optical light curves beyond $\phi = 0.75$. Additionally, irradiation feedback (Wadiasingh et al., 2018) and physical conditions within the stellar-wind shock can influence the results. The phenomenological IBS model presented here provides a foundation for understanding optical variability, but further investigation using physics-based models is warranted. Such a model can be further tested through both optical photometry and spectroscopy.

ACKNOWLEDGMENTS

JP acknowledges support from Basic Science Research Program through the National Research Foundation of Korea

(NRF) funded by the **Ministry of Education** (*RS-2023-00274559*). This research was supported by the National Research Foundation of Korea (NRF) grant funded by the **Korean Government (MSIT)** (*NRF-2023R1A2C1002718*).

REFERENCES

Alpar, M. A., Cheng, A. F., Ruderman, M. A., & Shaham, J. (1982, December), *Nature*, 300, 728-730.

An, H. (2022, January), ApJ, 924(2), 91.

An, H., & Romani, R. W. (2017, April), ApJ, 838, 145.

An, H., Romani, R. W., Johnson, T., Kerr, M., & Clark, C. J. (2017, November), ApJ, 850, 100.

An, H., Romani, R. W., & Kerr, M. (2018, Nov), ApJ, 868(1), L8.

An, H., Romani, R. W., & Kerr, M. (2020, July), ApJ, 897(1), 52.

Bogdanov, S., Esposito, P., Crawford, I., Fronefield, Possenti, A.,
McLaughlin, M. A., & Freire, P. (2014, January), ApJ, 781(1), 6.
Canto, J., Raga, A. C., & Wilkin, F. P. (1996, October), ApJ, 469.

Canto, J., Raga, A. C., & Wilkin, F. P. (1996, October), ApJ, 469, 729.

Caputo, R., Perkins, J., Racusin, J. et al. (2022, April), AMEGO-X Mission Overview. In AAS/High Energy Astrophysics Division Vol. 54, p. 404.03.

Clark, C. J., Nieder, L., Voisin, G. et al. (2021, March), *MNRAS*, 502(1), 915-934.

de Martino, D., Papitto, A., Belloni, T. et al. (2015, December), MNRAS, 454(2), 2190-2198.

Diplas, A., & Savage, B. D. (1994, May), ApJ, 427, 274.

Harding, A. K., & Gaisser, T. K. (1990, August), ApJ, 358, 561.

Hui, C. Y., Tam, P. H. T., Takata, J. et al. (2014, January), *ApJ*, 781(1), L21.

Kandel, D., Romani, R. W., & An, H. (2019, Jul), ApJ, 879(2), 73.

Kim, J., An, H., & Mori, K. (2022, September), ApJ, 936(1), 32.

Kong, A. K. H., Hui, C. Y., Takata, J., Li, K. L., & Tam, P. H. T. (2017, April), *ApJ*, *839*(2), 130.

Linares, M. (2020, December), Super-Massive Neutron Stars and Compact Binary Millisecond Pulsars. In Multifrequency Behaviour of High Energy Cosmic Sources - XIII. 3-8 June 2019. Palermo p. 23.

Linares, M., & Kachelrieß, M. (2021, February), J. Cosmology Astropart. Phys., 2021(2), 030.

Ng, C. W., Takata, J., Strader, J., Li, K. L., & Cheng, K. S. (2018, Nov), *ApJ*, 867(2), 90.

Romani, R. W., & Sanchez, N. (2016, September), ApJ, 828(1), 7.Ruderman, M. A., & Sutherland, P. G. (1975, February), ApJ, 196, 51-72.

Sim, M., An, H., & Wadiasingh, Z. (2024, April), *ApJ*, *964*(2), 109. Strader, J., Swihart, S., Chomiuk, L. et al. (2019, February), *ApJ*, *872*(1), 42.

Swihart, S. J., Strader, J., Chomiuk, L., Aydi, E., Sokolovsky, K. V., Ray, P. S., & Kerr, M. (2022, December), *ApJ*, 941(2), 199.

van der Merwe, C. J. T., Wadiasingh, Z., Venter, C., Harding, A. K., & Baring, M. G. (2020, December), *ApJ*, *904*(2), 91.

van Kerkwijk, M. H., Breton, R. P., & Kulkarni, S. R. (2011, February), *ApJ*, 728(2), 95.

Wadiasingh, Z., Harding, A. K., Venter, C., Böttcher, M., & Baring, M. G. (2017, April), ApJ, 839(2), 80.

Wadiasingh, Z., Venter, C., Harding, A. K., Böttcher, M., & Kilian, P. (2018, Dec), ApJ, 869(2), 120.